Journal of Aerosol Science 90 (2015) 1–13

Contents lists available at ScienceDirect

Journal of Aerosol Science

journal homepage: www.elsevier.com/locate/jaerosci

Technical note

Extrapolating particle concentration along the size axis in the nanometer size range requires discrete rate equations

Tinja Olenius [a,*], Oona Kupiainen-Määttä [a], Kari E.J. Lehtinen [b], Hanna Vehkamäki [a]

[a] Department of Physics, University of Helsinki, Gustaf Hällströmin katu 2 A, P.O. Box 64, FIN-00014 Helsinki, Finland
[b] Department of Applied Physics, University of Eastern Finland and Atmospheric Research Centre of Eastern Finland, Finnish Meteorological Institute, P.O. Box 1627, FIN-70211 Kuopio, Finland

ARTICLE INFO

Article history:
Received 29 April 2015
Received in revised form
3 July 2015
Accepted 15 July 2015
Available online 10 August 2015

Keywords:
Particle distribution
Modeling
Discrete general dynamic equation
Continuous general dynamic equation
New particle formation

ABSTRACT

For modeling or data analysis purposes, the concentration of atmospheric aerosol particles measured or modeled at a certain size is often extrapolated to a different size along the particle size axis. This is normally done using compact analytical formulae which are based on the assumption that particles of the same size move synchronously together in size space at the same rate, and thus a monodisperse population is not allowed to disperse. However, in reality the individual uncorrelated collision processes with vapor molecules introduce natural spreading to the particle distribution, which is fundamentally described by a set of discrete rate equations for each particle size. In the present work, predictions based on synchronous growth are compared to the results of the discrete treatment in the free molecular regime for particles of circa 1.5–3.3 nm in mass diameter in a situation where the population is affected by irreversible vapor condensation and scavenging losses. The comparison demonstrates that the results given by approaches that do not consider the discrete nature of the growth process may be distorted. In the studied cases, the differences to the discrete result are a factor of less than around ten, and the deviations are larger for faster particle formation events and often also for higher particle loss rates. Therefore, the discrete treatment should be used for obtaining reliable estimates on the size-dependent concentration of nanometer-sized particles.

1. Introduction

Exploring the growth dynamics of freshly formed aerosol particles has been the topic of numerous studies on atmospheric new particle formation. For some experimental data analysis or modeling purposes, the concentration or formation rate observed or modeled at a specific particle size needs to be extrapolated to another size. These purposes include testing the agreement between experimental particle formation rates and molecular clustering models by extrapolating the observed rate to a size smaller than what can be detected (*e.g.* Kerminen & Kulmala, 2002; Kürten, Williamson, Almeida, Kirkby, & Curtius, 2015), or providing input for models that do not include very small particles by

* Corresponding author. Current address: Department of Environmental Science and Analytical Chemistry (ACES) and Bolin Centre for Climate Research, Stockholm University, SE-10691 Stockholm, Sweden. Tel.: +46 8 674 7282.
E-mail address: tinja.olenius@aces.su.se (T. Olenius).

http://dx.doi.org/10.1016/j.jaerosci.2015.07.004
0021-8502/

extrapolating a formation rate predicted at a small size (where for example determining cluster properties from quantum chemistry is feasible) to a larger size that is treated by the model (*e.g.* Lee, Pierce, & Adams, 2013; Spracklen et al., 2006). Extrapolation can also be applied to generally assess the survival probability of small particles to larger, climatically relevant sizes.

Various studies have discussed the extrapolation of particle concentration along the size axis considering growth by vapor condensation and removal of particles due to external scavenging (see *e.g.* Lehtinen, Dal Maso, Kulmala, & Kerminen, 2007; Kerminen & Kulmala, 2002; Kerminen, Anttila, Lehtinen, & Kulmala, 2004; Kürten et al., 2015; Weber et al., 1997). Sometimes the condensational growth rate includes an estimated evaporation rate of molecules from the particle surface. In general the evaporation rate, which may be affected by complex chemistry in the particle phase, is considerably more difficult to assess than the molecular collision rate, calculated from gas kinetics. Thus, in many cases the assumption of irreversible condensation has been made to obtain an upper-limit estimate for the growth rate. This assumption is also justified if the vapors responsible for the major growth of stabilized particles are very low-volatile, as often suggested (Ehn et al., 2014; Kulmala et al., 2013). The effect of self-coagulation processes among the population of growing particles has often been assumed to be negligible in many atmospheric situations (Lehtinen et al., 2007; Kerminen and Kulmala, 2002), as the phenomenon is likely to become significant only at relatively high particle concentrations (Anttila, Kerminen, & Lehtinen, 2010; Kürten et al., 2015).

In most extrapolation approaches, including the widely applied Kerminen-Kulmala equation (Kerminen & Kulmala, 2002), all particles of the same size are approximated to change their size at the same rate. In other words, if a subset of particles is monodisperse at a given time, it will remain monodisperse as the particles grow, since each particle is assumed to move along the size axis at the same size-specific pace. However, in reality the growth occurs due to addition of individual molecules to the particles, and thus a more fundamental description of the process is provided by discrete rate equations (*e.g.* Goodrich, 1964a, 1964b). In this approach, each particle size, defined by the molecular content, is examined separately. The approximation of synchronous growth enormously simplifies the mathematical treatment of the problem, as analytical solutions to the set of discrete equations, even in cases where they exist, are often extremely complex (see *e.g.* Goodrich, 1964a, 1964b), and may not be very useful as such. However, the discrete collision processes may cause significant spreading in the size distribution, which decreases the concentration at a given size compared to the synchronous result. The spreading also affects the effective growth rate driving particles to larger sizes (Wang, McGraw, & Kuang, 2013).

The spreading of the particle size distribution, also referred to as size diffusion, has been studied in the past in terms of moment equations, which describe the mean particle size and the variance (Clement & Wood, 1979, 1980; Clement, Lehtinen, & Kulmala, 2004; Goodrich, 1964a). Previous work has addressed the width of the size distribution versus the mean size mostly for the case of a growing particle population with no external sources or sinks (see *e.g.* Clement & Wood, 1979; Clement et al., 2004). The relative spreading is often expected to become less significant as the mean size increases, but for some specific functional forms of a size-dependent condensation rate (Clement & Wood, 1979) or for a case where particles also evaporate (Clement et al., 2004), the spreading may be prominent even at large sizes. The effect of the discrete collisions has been recognized also in cloud droplet studies. Telford (1955) and Twomey (1964) studied the evolution of a droplet size spectrum in the absence of external sinks, and pointed out that the widening leads to a fraction of the growing cloud droplets reaching sizes larger than predicted by assuming that the droplets grow synchronously. In the context of particle formation, on the other hand, efforts have mainly been made to examine whether the width of the population remains narrow enough for the approximation of a sharp peak to be justified, and the effect of the widening on the particle number concentration within a given size interval has not received as much attention. However, concentration is the main focus of interest for instance when assessing the fraction of particles surviving to larger sizes. In the presence of a size-dependent particle sink, the effective particle loss rate is affected by the widening, and estimates of the survival probability based solely on the mean size of the population may be distorted.

The present work applies a discrete particle model to explore the validity of the approximation of synchronous growth on the size-dependent particle concentration. A population of growing particles in the size range of circa 1.5–3 nm in mass diameter is simulated with molecular resolution by numerically solving the set of discrete rate equations, and the results are compared to the simplified synchronous predictions. The focus is on a case where the only dynamic processes affecting the population are irreversible vapor condensation and scavenging losses. It must be noted that several studies (Sihto et al., 2006; Riipinen et al., 2007) have extrapolated the particle formation rate, defined as the number of particles grown into a certain size per unit time, instead of the particle number concentration studied in this work. However, extrapolation approaches have very often been applied to experimental data, and the directly measurable quantity is the concentration, from which the formation rate is deduced using estimated condensation and loss rates (Kulmala et al., 2012) or with some other method (*e.g.* Glasoe et al., 2015). Therefore, examining the concentration is considered more fundamental.

2. The discrete and continuous approaches to describe the time evolution of a particle population

The discrete equations for describing the condensational growth of a particle population in the presence of external sinks, as well as corresponding equations in which the particle size is approximated as a continuous variable, are briefly reviewed below. The result given by the continuous approximation, with certain assumptions (see below), is very likely the basis for the widely spread conception that a subset of particles of the same size retains its monodispersity as the particles grow. The discrete approach refers to explicitly considering each particle size consisting of a different number of molecules,

and describing the growth by the flux of particles between different sizes. The continuous approach follows from the discrete treatment by approximating the particle size and the concentration density along the size axis as continuous variables. In other words, there is no discretization based on the exact molecular content, but instead the concentration density is a differentiable function defined for all values describing the size. In principle, the effect of the approximation can be studied considering only condensational growth and neglecting the sinks. However, the focus of this work is on atmospheric situations, in which external sinks are always present and may have a significant effect on the particle population. Thus the sinks are included in the main analysis.

The discrete growth process through the condensation of individual vapor molecules is fundamentally described by a set of rate equations for each particle size. Each size i, defined by the molecular content, is treated separately, and the time derivative of the concentration C_i of size i is

$$\frac{dC_i}{dt} = f_{i-1}C_{i-1} - f_iC_i - S_iC_i, \tag{1}$$

where f_i and S_i are the condensation and loss coefficients of size i, respectively. The first term on the right-hand side corresponds to a source of size i due to growth from the previous size $i-1$, and the second and third terms describe the losses through growth to the subsequent size $i+1$ and to a scavenging sink, respectively. The discrete equations are, however, very difficult – or in many cases even impossible – to solve analytically except for very simple situations, and the time evolution of the concentrations for the discrete approach is most conveniently solved numerically. To simplify the problem when analytical estimates are desired, a continuous approximation has been applied to Eq. (1):

$$\left(\frac{\partial C(i,t)}{\partial t}\right)_i = f(i-1)C(i-1,t) - f(i)C(i,t) - S(i)C(i,t) \tag{2}$$

where the concentration density $C(i,t)$ is now a two-dimensional continuous function of particle size and time, and $f(i)$ and $S(i)$ are continuous functions of size. Integrating the concentration density over a range including exactly one particle size i would give the concentration C_i of size i as defined in Eq. (1). In order to obtain an equation where all terms are evaluated at the same size i and time t, the first term on the right hand side of Eq. (2) can be approximated by a first-order Taylor expansion with respect to the particle size to yield (see *e.g.* Brock, 1972; Lehtinen et al., 2007; Pich, Friedlander, & Lai, 1970; Ramabhadran, Peterson, & Seinfeld, 1976; Shi & Seinfeld, 1990)

$$\left(\frac{\partial C(i,t)}{\partial t}\right)_i = -\left(\frac{\partial (f(i)\times C(i,t))}{\partial i}\right)_t - S(i)C(i,t). \tag{3}$$

The first-order approximation Eq. (3) is the most widely used form of a continuous approach for the time-dependent particle size distribution, often referred to as the continuous general dynamic equation (GDE), in this case, however, with terms only for condensation and loss. It should be noted that in continuous approaches the particle size and the condensational growth coefficient are often expressed as the diameter and its change rate. As the quantity characterizing the size is a matter of convention, the molecular content is used here for a more straightforward comparison with the discrete equations. It should be kept in mind, though, that when approximating the size as a continuous variable, the molecular content can have non-integer values.

Eq. (3) can be solved more easily than the discrete equations (Eq. (1)) even for situations involving, for instance, size-dependent condensation or loss rates. However, there is a fundamental difference between the solutions obtained by the two approaches. To demonstrate this, the particle distribution is now solved for a simple example case of an initially monodisperse distribution with no additional particle sources. As analytical solutions to the discrete set of equations with size-dependent f and S are very complex (see *e.g.* Clement & Wood, 1979), size-independent rate constants, for which a compact analytical solution is found, are used in the below example for easier examination of the results.

For the discrete approach, the time-dependent concentrations can be solved from Eq. (1) recursively with the boundary conditions $C_i\,(t=0)=C_0(>0)$ for the smallest size $i=1$, and $C_i(t=0)=0$ for the larger sizes $i>1$. The time derivative of the concentration for size $i=1$ equals $-(f+S)C_1$, which gives $C_1(t)=C_0\exp[-(f+S)t]$ for the time-dependent concentration. For size $i=2$, $dC_2/dt=fC_1-(f+S)C_2$, resulting in $C_2(t)=C_0ft\exp[-(f+S)t]$. Continuing in a similar manner gives the time-dependent concentration of each particle size i:

$$C_i(t) = C_1(t=0)\frac{(ft)^{i-1}}{(i-1)!}\exp\left[-(f+S)t\right]. \tag{4}$$

The general result for the first-order continuous approach with size-independent condensation and loss coefficients f and S, on the other hand, is (see *e.g.* Olver, 2014 for the solution by the method of characteristics)

$$C(i,t) = F(i-ft)\exp(-St), \tag{5}$$

where F is the distribution function at $t=0$. From Eq. (5), it can be directly seen that the shape of F is preserved as the population grows, and the distribution is merely shifted along the size axis by the term ft. Therefore, if a particle population is monodisperse at some moment in time, it will remain monodisperse and all particles will grow at the same rate. Any size dependence of the condensation and loss rates would lead to the same conclusion that a monodisperse distribution retains its monodispersity; only the size-dependence of the growth rate would be different. However, a comparison of Eq. (5) with Eq. (4) shows that an important aspect of the true time evolution has been lost: in reality, the size distribution broadens.

Eq. (4) resembles the Poisson distribution, and it is obvious that the distribution along the size axis spreads significantly as t increases. For instance, in the most simple case with no external losses $S=0$, for a condensation frequency of $f=10^{-2}\ \mathrm{s}^{-1}$, 99% of the initial population $C_1(t=0)$ are still in the smallest size $i=1$ after one second. After ten seconds, 90% of the particles remain at size $i=1$; 9% have shifted to size $i=2$, and 0.5% to size $i=3$, and so on. After one minute, the corresponding percentages are 55%, 33%, and 10%. Eq. (5), on the other hand, gives a sharp peak that moves along the size axis according to the growth rate f retaining its original height, and is found at sizes $i=1.01$, 1.1, and 1.6 after one second, ten seconds and one minute, respectively. The widening of a sharp distribution peak in the absence of sinks has been studied in more detail by, for instance, Clement and Wood (1979) and Clement et al. (2004).

The reason for the absence of broadening in Eq. (5) originates from the first-order approximation made in Eq. (3). Including a second order term in the Taylor expansion of Eq. (2) results in the equation

$$\left(\frac{\partial C(i,t)}{\partial t}\right)_i = -\left(\frac{\partial (f(i)\times C(i,t))}{\partial i}\right)_t + \frac{1}{2}\left(\frac{\partial^2 (f(i)\times C(i,t))}{\partial i^2}\right)_t - S(i)C(i,t). \tag{6}$$

The second order term can be seen as a diffusion term that smoothens gradients in size space, thus spreading sharp distributions. Eq. (6) can be solved by the methods of Fourier transform or Green's function (see *e.g.* Olver, 2014; Precup, 2013). The solution for a population that is monodisperse at size $i=1$ at time $t=0$ in the case of size-independent rate constants is

$$C(i,t) = C_1(t=0)(2\pi f t)^{-\frac{1}{2}} \exp\left[-\frac{(i-1)^2}{2ft} + (i-1) - \left(\frac{f}{2}+S\right)t\right], \tag{7}$$

which does include spreading along the size axis. In fact, the distribution given by Eq. (7) is very close to the solution of the discrete problem (Eq. (4)), although the differences slightly increase with increasing S/f ratio (Fig. A1 in the appendix; see also Noppel, 1996). However, Eq. (6) is not easily solved for size-dependent rate constants, and in practice the term including the second derivative has been assumed to be negligible (see *e.g.* Brock, 1972; Ramabhadran et al., 1976).

3. The monodisperse mode and first-order continuous approaches to extrapolate particle concentration

The assumption of synchronous growth introduced in the previous Section is the basis for established approaches to extrapolate particle concentration along the size axis (Lehtinen et al., 2007; Kerminen & Kulmala, 2002; Weber et al., 1997). Probably the most widely known and cited work on this type of extrapolation is that by Kerminen and Kulmala (2002) in which a formula for size-dependent particle concentration is derived; a similar result has been presented by Weber et al. (1997). The result slightly deviates from that of the first-order continuous approximation solved for a steady state (Lehtinen et al., 2007; see Eq. (14) below), and thus the formula by Kerminen and Kulmala (2002) will be from now on referred to as the monodisperse mode approach in order to distinguish between the two.

The derivation of the monodisperse mode approach is reviewed below. Since in the original derivation the particle size is characterized by the diameter, the same convention is used in the review. Otherwise, the size is expressed as the number of molecules (in other words, the particle mass) as this is more practical for the comparison with the discrete size distribution with molecular size resolution. For the same reason, the rate at which the particles grow due to vapor condensation, often expressed as the change in the particle diameter per unit time, is here characterized by the frequency at which the particle gains vapor molecules, *i.e.* the number of collisions per unit time. When using the latter convention, the condensation rate also has the same unit (s^{-1}) as the external loss rate, making the comparison of the time scales easier.

The result for the monodisperse mode approach (Kerminen & Kulmala, 2002) was originally derived assuming a rapid particle formation burst which produces a monodisperse population of new nuclei. The freshly formed particles are assumed to grow by vapor condensation at a diameter change rate of $\mathrm{d}d_\mathrm{p}/\mathrm{d}t \equiv \mathrm{GR}$, while at the same time being lost on pre-existing larger particles. The loss rate is assumed to depend on particle size, but not to vary in time during the growth event. At a given moment in time, all particles have the same size d_p, but this size increases with time. The particle concentration as a function of size is derived by first writing the time derivative of the particle concentration C as (Kerminen & Kulmala, 2002)

$$\frac{\mathrm{d}C}{\mathrm{d}t} = -SC, \tag{8}$$

where S is again the size-dependent loss coefficient corresponding to the scavenging sink, evaluated at the size d_p corresponding to time t. The left-hand side of Eq. (8) is then re-written as

$$\frac{\mathrm{d}C}{\mathrm{d}t} = \frac{\mathrm{d}C}{\mathrm{d}d_\mathrm{p}}\frac{\mathrm{d}d_\mathrm{p}}{\mathrm{d}t} = \frac{\mathrm{d}C}{\mathrm{d}d_\mathrm{p}}\mathrm{GR}, \tag{9}$$

and the concentration $C(d_\mathrm{p})$ is solved from the resulting differential equation

$$\frac{\mathrm{d}C}{\mathrm{d}d_\mathrm{p}} = -\frac{S}{\mathrm{GR}}C. \tag{10}$$

Integration from an initial size $d_{p,1}$ to a larger size $d_{p,2}$ yields the final result

$$C(d_{p,2}) = C(d_{p,1})\exp\left(- \int_{d_{p,1}}^{d_{p,2}} \frac{S}{\mathrm{GR}} \mathrm{d}d_p \right), \tag{11}$$

where the integral can be evaluated when the rate coefficients GR and S are known. The original derivation assumes a constant GR, but a size dependence can naturally be included in the integrand, as the derivation of Eq. (10) does not involve any assumptions about the size-dependence of GR. Eq. (11) can be written by characterizing the size by the number of molecules n as

$$C(n_2) = C(n_1)\exp\left(- \int_{n_1}^{n_2} \frac{S}{f} \mathrm{d}n \right), \tag{12}$$

where the change rate of the molecular content is denoted by $\mathrm{d}n/\mathrm{d}t \equiv f$. The central idea of the monodisperse mode treatment (Eqs. (8)–(12)) is that at each moment, the distribution is characterized by a single value for the particle size, and thus the time dependence of the particle concentration can be converted into a size dependence as in Eq. (9).

It is in order to acknowledge that for a steady state, an extrapolation based on the first-order continuous approximation (Eq. (3)) has been presented by Lehtinen et al. (2007) in terms of particle formation rate, defined as $J(i) \equiv f(i) \times C(i)$. Setting the time derivative on the left-hand side of Eq. (3) to zero leads to equation $\mathrm{d}J/\mathrm{d}i = -S/f \times J$ (in the original derivation by Lehtinen et al. (2007) this is written using the diameter as the size variable: $\mathrm{d}J/\mathrm{d}d_p = -S/\mathrm{GR} \times J$), which can be readily integrated to yield

$$J(n_i) = J(n_1)\exp\left(- \int_{n_1}^{n_i} \frac{S}{f} \mathrm{d}n \right). \tag{13}$$

The form of Eq. (13) is similar to Eq. (12), except that the former is given for particle formation rate, and the latter for particle number concentration. In fact, in the original work by Kerminen and Kulmala (2002), concentrations C are simply replaced with formation rates J after deriving Eq. (11), leading to the same result as in the continuous approximation (Eq. (13)). However, it is obvious that if the formation rate is defined as $J = f \times C$, the concentration C in Eq. (12) cannot be replaced by formation rate J in the case of a size-dependent condensation coefficient f, as the right-hand side and left-hand side of Eq. (12) would be multiplied by different numbers. Eq. (13) can be written in terms of concentrations as

$$C(n_i) = C(n_1)\frac{f_1}{f_i}\exp\left(- \int_{n_1}^{n_i} \frac{S}{f} \mathrm{d}n \right). \tag{14}$$

The result differs from that of the monodisperse mode treatment (Eq. (12)) by a factor of f_1/f_i, which becomes prominent when the condensation coefficient f varies significantly in the studied size range. It must, however, be noted that at least in principle in the monodisperse mode case the concentrations at different sizes correspond to different points in time, while in the first-order continuous approximation particles of all sizes are present at the same time. Results given by Eq. (14) are also presented in the comparison with the discrete approach, since Eq. (14) has been applied in studies involving extrapolation (Korhonen, Sihto, Kerminen, & Lehtinen, 2011; Korhonen, Kerminen, Kokkola, & Lehtinen, 2014), and its derivation differs from that of the formula by Kerminen and Kulmala (2002) (Eq. (11)). Although Eq. (14) was originally derived for a steady state, it has been used also for time-dependent situations by applying a time shift determined by the condensation rate (see Eqs. (19) and (20) below; Korhonen et al., 2014). The time shift is also introduced in the work by Kerminen and Kulmala (2002).

4. Application of the monodisperse mode and first-order continuous approaches to situations with different time dependencies

The following sections discuss a simple case of particle growth where vapor molecules condense onto initial core particles. Sections 4.2–4.4 consider different scenarios for the time dependence of the particle concentrations, but in all the cases the only processes considered are growth by condensation and losses to external surfaces. The particle concentration is extrapolated from a small initial size towards larger sizes, but the extrapolation can of course be performed into either direction along the size axis (an example of extrapolation from a large size to smaller sizes is shown in Appendix A).

4.1. Rate constants used in the calculations

In the presented example cases, the collision frequency between a vapor molecule and a particle of size i is calculated as in kinetic gas theory assuming that the particle is considerably larger than the vapor molecule (see *e.g.* Chapman & Cowling, 1970)

$$f_i = C_{\mathrm{vapor}}\left(\frac{k_B T}{2\pi m_{\mathrm{vapor}}}\right)^{1/2} A_i, \tag{15}$$

where C_{vapor} and m_{vapor} are the vapor concentration and mass, respectively, k_B is the Boltzmann coefficient, T is the temperature, and A_i is the surface area of the particle. For simplicity, the molecules of the initial core particle are assumed to

have the same mass and liquid density as the molecules of the condensing vapor, and thus A_i is

$$A_i = \pi^{1/3}\left(\frac{6m_{\text{vapor}}}{\rho_{\text{liquid}}}n_i\right)^{2/3}, \tag{16}$$

where ρ_{liquid} is the liquid density of the condensing substance, and n_i is the total number of molecules in the particle. Therefore the size-dependent collision frequency (Eq. (15)) can be written as $f_i = f' n_i^{2/3}$, where f' is a constant. In this work, ρ_{liquid} is assumed to be 1 g cm^{-3}, and m_{vapor} is assumed to be 100 amu, which is around the mass of atmospheric species that are assumed to participate in the condensational growth of small particles, such as sulfuric acid and some organic compounds (see *e.g.* Schobesberger et al., 2013; Zhang et al., 2004). The temperature is set to 278 K. The particles are assumed to consist of ten core molecules and 0–100 condensing vapor molecules, corresponding to the size range of 1.5–3.3 nm in mass diameter. This results in collision frequencies f_i ranging from 4×10^{-3} s^{-1} to 2×10^{-2} s^{-1} when the concentration of the condensing vapor is $C_{\text{vapor}} = 10^7$ cm^{-3}. This corresponds to a mass diameter growth rate of circa 0.73 nm h^{-1}, calculated as $\mathrm{d}d_{\text{p}}/\mathrm{d}t = \mathrm{d}d_{\text{p}}/\mathrm{d}V_{\text{p}} \times \mathrm{d}V_{\text{p}}/\mathrm{d}t$, where $\mathrm{d}V_{\text{p}}/\mathrm{d}t = \rho_{\text{liquid}}^{-1}\,\mathrm{d}m_{\text{p}}/\mathrm{d}t = \rho_{\text{liquid}}^{-1}\, m_{\text{vapor}} f$ and the subscript p refers to the particle. Decreasing or increasing the condensation rate constants by a factor of two did not alter the qualitative results.

The loss frequency of a particle of a diameter of $d_{\text{p},i}$ is approximated as (Lehtinen et al., 2007)

$$S_i = S_{\text{ref}}\left(\frac{d_{\text{p},i}}{d_{\text{p,ref}}}\right)^m = S_{\text{ref}}\left(\frac{n_i}{n_{\text{ref}}}\right)^{m/3}, \tag{17}$$

where S_{ref} is the sink of a reference size $d_{\text{p,ref}}$, and m is a constant. The last form of Eq. (17) follows from the assumption that the core molecules and the vapor molecules have equal molecular volumes. Here the reference size is taken to be the initial core particle, and m is set to -1.7, corresponding to a typical coagulational scavenging sink in a boreal forest environment (Lehtinen et al., 2007). S_{ref} is set to either 10^{-4} s^{-1} or 10^{-3} s^{-1}. In the studied size range, $S_{\text{ref}} = 10^{-4}$ s^{-1} results in loss frequencies decreasing from 10^{-4} s^{-1} to circa 3×10^{-5} s^{-1} with increasing particle size.

The concentration at size i in the monodisperse mode treatment is obtained by inserting Eqs. (15) and (17) in Eq. (12)

$$C(n_i) = C(n_1)\exp\left\{\frac{S_1}{f_1}\frac{3}{m+1}n_1\left[1-\left(\frac{n_i}{n_1}\right)^{(m+1)/3}\right]\right\}, \tag{18}$$

where the first particle $i=1$ is used as the reference size n_{ref} in Eq. (17). In the studied size range, the difference between the first-order continuous approximation (Eq. (14)), involving the pre-factor of f_1/f_i and the monodisperse mode approach increases with particle size up to a factor of 0.2 at $i=101$.

The time evolution of the distribution in the discrete approach is solved from the differential equations (Eq. (1)) with the ACDC code that uses the MATLAB ode15s solver (for more details, see *e.g.* Olenius, Riipinen, Lehtipalo, & Vehkamäki, 2014). The equations are solved for particles containing up to 100 vapor molecules, and particles that grow larger than the studied size range are removed from the simulation.

The functional forms of the rate constants f and S were chosen for a physically realistic size-dependence, and their orders of magnitude (in practice, C_{vapor} and S_{ref}) were set to be in the range of typical atmospheric values that favor particle formation events in the sense that a significant fraction of the population is expected to survive to larger sizes. Test simulations performed using size-independent f and S did not alter the qualitative results for the differences between the different approaches.

4.2. Initially monodisperse population with no additional sources

Figure 1 shows the comparison of the discrete (based on Eq. (1)), monodisperse mode (Eq. (12)) and first-order continuous (Eq. (14)) approaches for a population that is monodisperse at the smallest size $i=1$ at $t=0$, the situation for which the monodisperse mode extrapolation (Eq. (12)) is originally derived. Vapor concentration C_{vapor} and the reference size loss coefficient S_{ref} are set to 10^7 cm^{-3} and 10^{-4} s^{-1}, respectively. Thick solid lines show the time development of the concentrations of particles of different sizes solved from the discrete equations (Eq. (1)), and circles and diamonds depict the concentrations given by the monodisperse mode (Eq. (12)) and continuous (Eq. (14)) treatments, respectively. The markers are placed at time intervals $\Delta t_{\text{growth},i}$ at which the population is assumed to reach size i based on the growth rates f:

$$\Delta t_{\text{growth},i} = \int_{n_1}^{n_i}\frac{\mathrm{d}n}{f} = \frac{3}{f_1}n_1\left[\left(\frac{n_i}{n_1}\right)^{1/3}-1\right]. \tag{19}$$

When compared to the real time evolution of the concentration of each size given by the discrete treatment, the monodisperse mode approach clearly overestimates the concentrations, as expected, since it assumes that the height of the sharp distribution peak decreases solely due to scavenging losses and is not affected by the widening of the distribution in size space (see Fig. 2 for the size-dependent distribution at specific times). For example, the monodisperse mode prediction for the size of 100 vapor molecules is by a factor of 50 higher than the maximum concentration for that size. Concentrations predicted by the first-order continuous approximation are lower, but likewise too high compared to the discrete result as

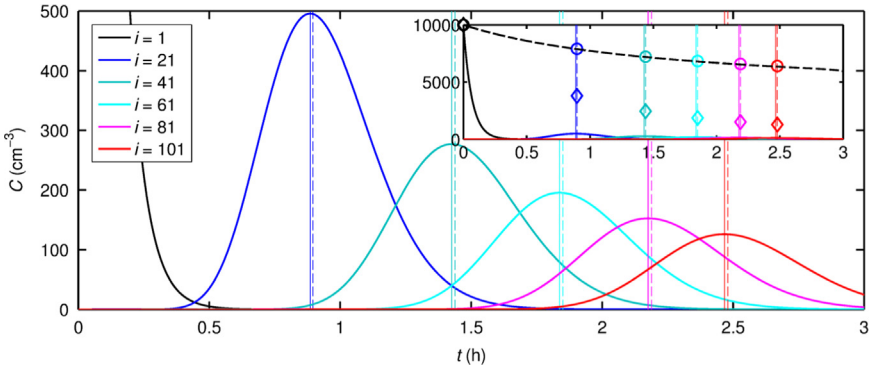

Fig. 1. Time evolution of the concentrations of particles containing 0–100 vapor molecules for an initially monodisperse distribution $C_i(t=0)=10^4$ cm^{-3} for $i=1$, and $C_i(t=0)=0$ for $i>1$. Vapor concentration C_{vapor} and the reference size loss coefficient S_{ref} are set to 10^7 cm^{-3} and 10^{-4} s^{-1}, respectively. Thick solid lines show the concentration of individual particle sizes $i=1, 21, 41,\ldots,101$ obtained from the discrete rate equations, and the dashed black line shows the evolution of the total concentration ΣC_i (note that here the simulation includes particles containing up to 200 vapor molecules in order to obtain correct ΣC_i when the majority of the population has reached larger sizes). Thin solid vertical lines show the times at which each size reaches its maximum concentration. For the same sizes, circles and diamonds depict the concentration obtained by the monodisperse mode (Eq. (12)) and first-order continuous (Eq. (14)) treatments, respectively, extrapolated from the initial concentration $C_1(t=0)$, and marked at times $\Delta t_{growth,i}$ (thin dashed vertical lines; Eq. (19)) at which the particles are assumed to reach size i. The main frame is a zoom to concentrations below 500 cm^{-3}, and the general view with concentrations up to 10^4 cm^{-3} is shown in the inset.

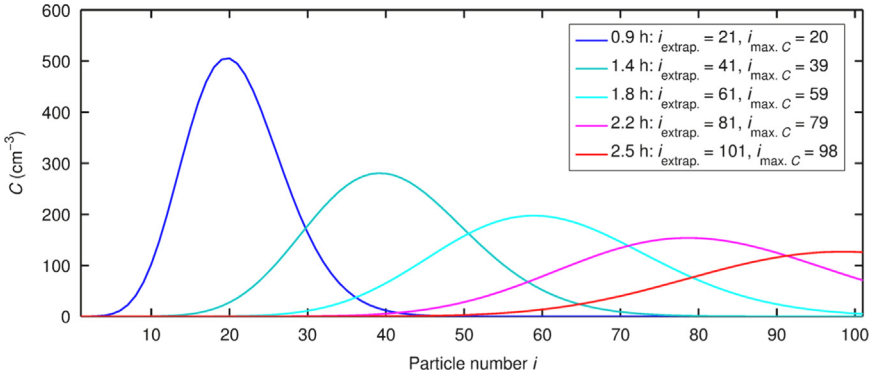

Fig. 2. Particle distribution solved from the discrete rate equations in the conditions of Fig. 1. The distribution is shown for the times $\Delta t_{growth,i}$ (Eq. (19)) at which the population is assumed to reach sizes $i_{extrap}=21, 41,\ldots,101$ according to the monodisperse mode and first-order continuous approaches. $i_{max.C}$ are the sizes corresponding to the maximum concentration along the size axis at these times according to the discrete solution.

the decreasing effect of the broadening is not considered. Figure 1 also shows that the growth times $\Delta t_{growth,i}$ (Eq. (19)) based on the assumption of no size dispersion do not exactly coincide with the times at which the time-dependent concentration at size i peaks.

It should be noted, though, that in the simulated conditions the monodisperse mode extrapolation agrees rather well with the total concentration ΣC_i, shown as dashed black line in Fig. 1. Here the simulation included particles containing up to 200 vapor molecules in order to obtain the correct total concentration. Particles larger than 200 vapor molecules did not in practice form in the simulation time of Fig. 1. The concentrations given by the continuous approximation, on the other hand, differ from the total concentration by down to a factor of 0.2. The agreement in the case of the monodisperse mode approach is likely due to the fact that the loss frequency given by Eq. (17) is a relatively weak function of size in the studied size range. Also, the agreement is not this good for all rate constant values; for instance, when the reference size loss coefficient S_{ref} is set to a higher value of 5×10^{-3} s^{-1}, the monodisperse mode extrapolation underestimates the total concentration by factors of 0.5 and 0.3 at the times when the sizes of 50 and 100 vapor molecules reach their maximum concentration, respectively. However, it should be kept in mind that the total concentration is not a relevant quantity when one wishes to assess the fraction of the initial particles that survive to a specific larger size.

Particle concentration as a function of size at specific times solved from the discrete equations is shown in Fig. 2. The times are the moments $\Delta t_{growth,i}$ (Eq. (19)) at which the population is assumed to reach sizes $i=21, 41,\ldots,101$ according to the simplified approaches. It is clear that the initially monodisperse distribution broadens significantly along the size axis. Furthermore, the size that the population is assumed to reach at $\Delta t_{growth,i}$ according to the simplified approaches does not exactly coincide with the size corresponding to the peak of the distribution.

In general, Figs. 1 and 2 demonstrate that the distribution dynamics are more complicated than can be captured by the simplified approaches. On the other hand, a rapid burst where a population of particles suddenly appears at some small size

may not be very relevant for atmospheric particle formation events. Instead, a situation involving a particle source at a small size, discussed in Section 4.3, may often be more realistic.

4.3. Time-dependent particle source

Atmospheric particle formation events, for which the simplified approaches have been applied in many studies (Sihto et al., 2006; Riipinen et al., 2007; Korhonen et al., 2014), often involve a time-dependent source of small particles due to the diurnal variation in the precursor vapor concentrations. Thus, the concentration of the "core" particle $i=1$ was set to follow a sinusoidal function from zero to π between times $t_{C1,\mathrm{start}}$ and $t_{C1,\mathrm{end}}$, and to zero elsewhere. The length of the formation period $t_{C1,\mathrm{end}}-t_{C1,\mathrm{start}}$ was set to either one or four hours and the peak value to $C_{1,\max}=10^4\ \mathrm{cm}^{-3}$, and the time evolution of the population $i>1$ was solved from the differential equations. The monodisperse mode and continuous approximations are applied taking into account the assumed growth time $\Delta t_{\mathrm{growth},i}$ from size 1 to size i (Eq. (19); Kerminen & Kulmala, 2002; Kerminen et al., 2004; Korhonen et al., 2014):

$$C_i(t+\Delta t_{\mathrm{growth},i}) = C_1(t) X \exp\left(-\int_{n_1}^{n_i} \frac{S}{f}\mathrm{d}n\right), \tag{20}$$

where X equals one and f_1/f_i for the monodisperse mode and continuous approaches, respectively.

Figure 3 presents particle concentrations as a function of time for the formation periods of one and four hours (upper and lower panels (a) and (b), respectively), and reference loss rates of $10^{-4}\ \mathrm{s}^{-1}$ (left-hand panels) and $10^{-3}\ \mathrm{s}^{-1}$ (right-hand panels). Figure A2 in Appendix A shows the results of an extrapolation from a large size towards smaller sizes for the same conditions, since experimental data has often been scaled to a size smaller than what can be detected (see *e.g.* Sihto et al., 2006). The comparison presented in Fig. 3 shows that the monodisperse mode treatment gives erroneous results for the absolute concentrations, and in addition, both the width of the time-dependent concentration curve C_i at size i and its location along the time axis are distorted. For instance, for a loss frequency of $10^{-4}\ \mathrm{s}^{-1}$, the prediction for the maximum concentration of the largest size of 100 vapor molecules differs from the discrete approach by factors of 6.8 and 5.0 for $t_{C1,\mathrm{end}}-t_{C1,\mathrm{start}}=1$ h and 4 h, respectively. The difference in the time at which the maximum value is reached deviates from the discrete results by a couple of minutes. For reference size loss coefficient $S_{\mathrm{ref}}=10^{-3}\ \mathrm{s}^{-1}$, the difference between the absolute concentrations is of the same order as for $S_{\mathrm{ref}}=10^{-4}\ \mathrm{s}^{-1}$, but the time deviation is circa ten minutes for both $t_{C1,\mathrm{end}}-t_{C1,\mathrm{start}}$.

The first-order continuous approximation, on the other hand, is very close to the discrete result for the formation period of four hours and $S_{\mathrm{ref}}=10^{-4}\ \mathrm{s}^{-1}$ (left-hand panel in Fig. 3b), but produces distorted predictions in the cases of more rapid time development (panel (a)) and higher loss rate $S_{\mathrm{ref}}=10^{-3}\ \mathrm{s}^{-1}$ (right-hand panels). The ratios of the peak

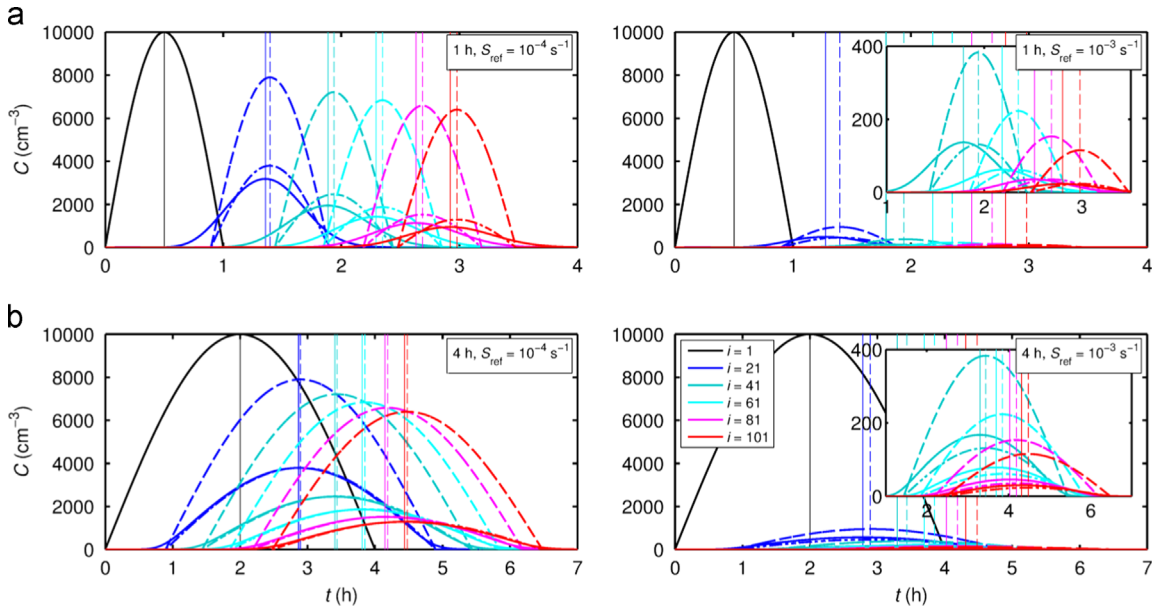

Fig. 3. Particle concentrations solved from the discrete rate equations as a function of time (thick solid lines), and the result given by the monodisperse mode formula (Eq. (12); thick dashed lines) and the first-order continuous approximation (Eq. (14); thick dash-dotted lines) shifted by the assumed growth time $\Delta t_{\mathrm{growth},i}$ (Eq. (19)) for a sinusoidal concentration $C_1(t)$ with a peak value of $10^4\ \mathrm{cm}^{-3}$ for the smallest size studied $i=1$. Thin vertical lines show the times at which each size reaches its maximum concentration according to the discrete (solid lines) and monodisperse mode and continuous (dashed lines) approaches. The formation period $t_{C1,\mathrm{end}}-t_{C1,\mathrm{start}}$ for which $C_1(t)>0$ is either one hour (panel (a)) or four hours (panel (b)). C_{vapor} is $10^7\ \mathrm{cm}^{-3}$, and the reference size loss coefficient S_{ref} is set to $10^{-4}\ \mathrm{s}^{-1}$ (left-hand panels) and $10^{-3}\ \mathrm{s}^{-1}$ (right-hand panels). The insets on the right-hand panels show enlargements for sizes $i>40$. For figure clarity, only the data for every 20th particle are shown.

concentrations of the largest simulated size obtained from the continuous and discrete treatments for the formation periods of one and four hours are 1.4 and 1.0 when S_{ref} is 10^{-4} s^{-1}, and 1.0 and 0.8 when S_{ref} is 10^{-3} s^{-1}, respectively. Thus, the continuous approximation can both over- or underestimate the absolute concentration depending on the conditions. The predicted time at which the peak concentration is reached for each size i is overestimated as in the case of the monodisperse mode approach, since the same time shift $\Delta t_{\mathrm{growth},i}$ is applied for both the continuous and the monodisperse mode treatments. Therefore, even when the predicted concentration is close to the discrete result, its location on the time axis may be incorrect, as is the case for $t_{C1,\mathrm{end}} - t_{C1,\mathrm{start}} = 1$ h and $S_{ref} = 10^{-3}$ s^{-1}. It must be noted that the difference to the discrete approach does not depend solely on the relative condensation and loss rates: for instance, if all the condensation and loss rate coefficients f and S are decreased by a factor of two or five in the case of $t_{C1,\mathrm{end}} - t_{C1,\mathrm{start}} = 4$ h and $S_{ref} = 10^{-4}$ s^{-1}, for which the first-order approximation coincides very well with the discrete result (left-hand panel in Fig. 3b), the peak concentration of the largest simulated size differs from the discrete result by factors of 1.1 and 1.6, respectively.

The qualitative comparison is similar for a more polluted environment with $S_{ref} = 2 \times 10^{-3}$ s^{-1} (not shown in the figure). The peak concentration of the largest size given by the monodisperse mode approach differs from the discrete result by factors of 2.7 and 2.1 for $t_{C1,\mathrm{end}} - t_{C1,\mathrm{start}} = 1$ h and 4 h, respectively. For the first-order continuous approximation, the corresponding relative differences are 0.55 and 0.43. The time at which the peak concentration is reached according to the simplified approaches is overestimated, however, by almost 20 min.

Figure 4 presents the particle distribution at different times in the conditions of Fig. 3. It can be seen that the monodisperse mode and continuous approximations predict a narrower distribution compared to the discrete result, with the absolute difference depending on the conditions. Moreover, the different approaches can also give different predictions for the location of the peak concentration on the size axis. The fact that the shape of the distribution varies for different times for the monodisperse mode and continuous approaches is not to be confused with the broadening originating from the discrete collision processes, which is here taken into account solely in the discrete approach. The simplified approaches still assume no broadening for a monodisperse subgroup, but the time-dependent particle source at the smallest size $i = 1$ and size-dependent rate constants give rise to the time evolution of the shape of the distribution. Nevertheless, the width of the distribution given by non-discrete approaches remains in general narrower than the discrete result, as discussed for example by Twomey (1964).

In order to better elucidate the effect of the discrete growth process on the time-dependent concentrations, a special case of a time-dependent situation corresponding to the conditions of Fig. 3 involving a size-independent condensation rate and no sinks is shown in Fig. 5. In this case, the size distribution broadens solely due to the discrete collisions with vapor molecules, since all sizes gain molecules at the same rate. In the absence of sinks, the peak concentration of each size $i > 1$ decreases compared to that of the first size $i = 1$ only because of the spreading. Therefore, this example case demonstrates a simple situation in which the discrete collisions are truly the only factor decreasing the size-specific concentration and altering the distribution. Note that here the monodisperse mode and continuous approaches give the same result because of the size-independent condensation rate f. For the formation period of $t_{C1,\mathrm{end}} - t_{C1,\mathrm{start}} = 1$ h (panel (a)), the effect of the

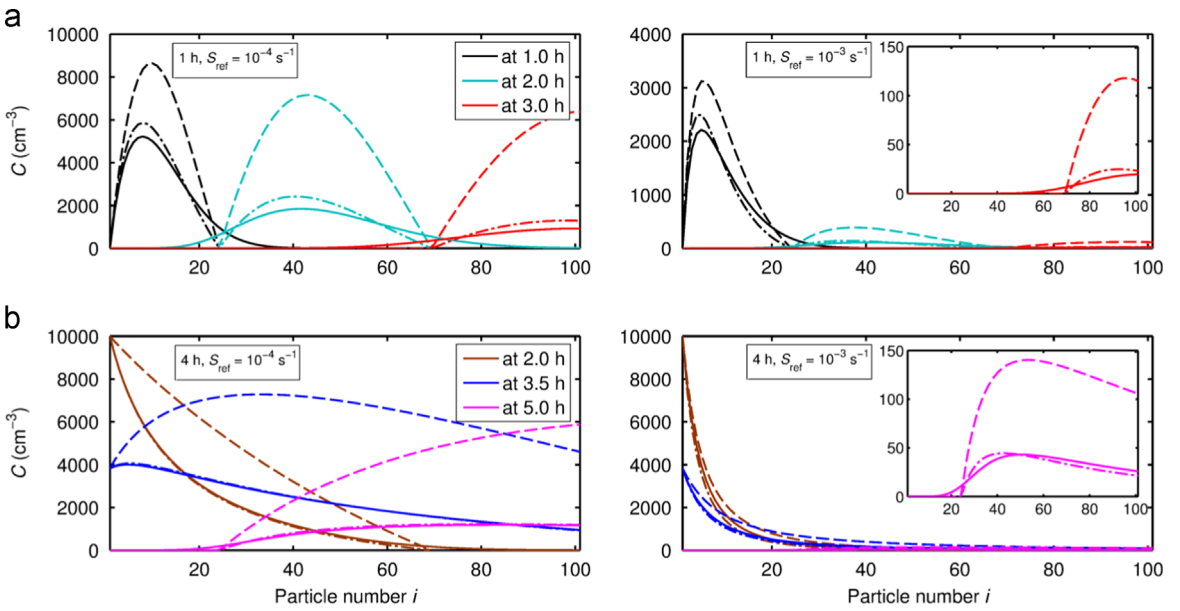

Fig. 4. Particle distribution at different times solved from the discrete rate equations (solid lines), the monodisperse mode approach (Eq. (12); dashed lines), and the first-order continuous approximation (Eq. (14); dash-dotted lines). Explanations for the panels are as in Fig. 3. The insets on the right-hand panels show enlargements for the times $t = 3$ h (panel (a)) and 5 h (panel (b)).

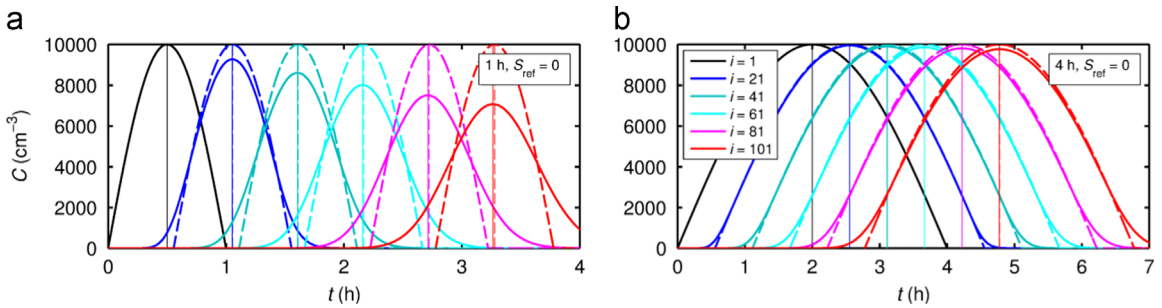

Fig. 5. Particle concentrations solved from the discrete rate equations as a function of time (thick solid lines), and concentrations extrapolated from the smallest size studied according to the monodisperse mode and first-order continuous approaches (Eq. (12); thick dashed lines), shifted by the assumed growth time $\Delta t_{\mathrm{growth},i}$ (Eq. (19)). The condensation rate f is set to a constant value of $10^{-2}\,\mathrm{s}^{-1}$ for all sizes, and no external sinks are used ($S=0$). The time period $t_{C1,\mathrm{end}}-t_{C1,\mathrm{start}}$ for which $C_1(t)>0$ is either one hour (panel (a)) or four hours (panel (b)).

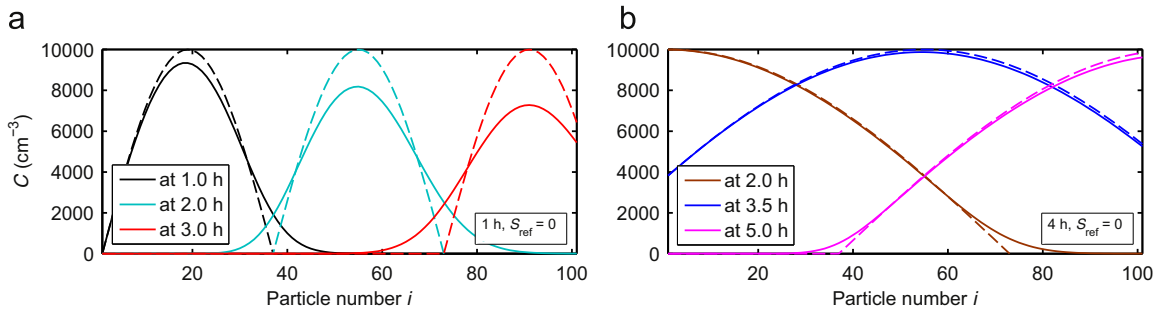

Fig. 6. Particle distribution at different times solved from the discrete rate equations (solid lines) and the monodisperse mode and first-order continuous approaches (Eq. (12); dashed lines). Explanations for the panels are as in Fig. 5.

broadening is prominent: the maximum concentration of the largest size $i=101$ is a factor of 0.71 lower than that of the first size. For the formation period of $t_{C1,\mathrm{end}}-t_{C1,\mathrm{start}}=4$ h (panel (b)), the difference is only a factor of 0.98. This is likely because the time scale of the time evolution at $i=1$ is considerably longer than that of the condensation process. If the condensation rate is decreased by a factor of two, for instance, the relative difference is 0.91. Figure 6 shows the spreading of the distribution along the size axis: for the shorter formation period, the widening is significant (panel (a)), while for the longer formation period its effect is small (panel (b)).

4.4. Steady state

An often studied straightforward special case is a time-independent steady state, corresponding to a constant particle source. In this case, concentrations given by the discrete treatment can simply be solved recursively from Eq. (1) as

$$C_{i+1}=\frac{f_i}{f_{i+1}+S_{i+1}}C_i. \tag{21}$$

Figure 7 shows the comparison of the simplified approaches to the accurate discrete treatment for a steady-state distribution. While the continuous approximation is again close to the discrete result for $S_{\mathrm{ref}}=10^{-4}$ (black lines), the prediction of the monodisperse mode approach is off by up to a factor of 5. It must be noted that the monodisperse mode treatment is not entirely consistent for a steady state, although the distribution could be understood as an infinite number of monodisperse subsets that are fed to the smallest size at a constant rate. For a situation with no external losses $S=0$, Eq. (12) gives equal concentration for all particle sizes. For size-dependent condensation coefficient f, this conflicts with the fact that the flux $J=f\times C$ must be constant throughout the size range in the absence of sinks.

When all the loss coefficients are increased by a factor of ten ($S_{\mathrm{ref}}=10^{-3}$), the continuous approximation deviates more from the discrete concentrations (in the given conditions by down to a factor of 0.8; magenta lines). This can be easily reasoned in a simplified way by examining the ratio of the concentrations of two subsequent particles, assuming that the rate constants are approximately equal for the adjacent sizes. Eq. (20) then gives the ratio as $C_{i+1}/C_i=\exp(-S/f)$. For small S/f, this can be further approximated as $\exp(-S/f)\approx(1+S/f)^{-1}=f/(f+S)$, which equals the discrete result (Eq. (21)). Thus the difference between the differential approximation and the discrete solution can be expected to increase with increasing S/f. For instance, for a reference loss rate of $2\times10^{-3}\,\mathrm{s}^{-1}$, the deviation is down to a factor of circa 0.4.

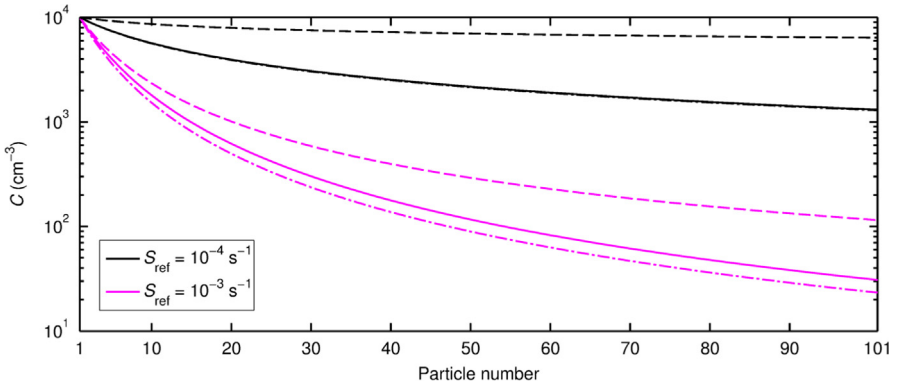

Fig. 7. Discrete steady-state distribution (Eq. (21); solid lines) and the results of the monodisperse mode treatment (Eq. (12); dashed lines) and the first-order continuous approximation (Eq. (14); dash-dotted lines) for vapor concentration $C_{vapor} = 10^7$ cm^{-3}, and loss frequencies calculated with $S_{ref} = 10^{-4}$ s^{-1} (black) and $S_{ref} = 10^{-3}$ s^{-1} (magenta). Note that the black solid and dash-dotted lines fall on top of each other. (For interpretation of the references to color in this figure legend, the reader is referred to the web version of this article.)

5. Conclusions

Size-dependent concentration of particles in the size range of 1.5–3.3 nm in mass diameter was solved (1) from the fundamental discrete rate equations describing each particle size separately, and (2) by applying an often used assumption that particles of the same size grow synchronously at the same rate, and thus a monodisperse population is not allowed to disperse. The results of the different approaches were compared in a case where the particle population is affected solely by irreversible vapor condensation and external particle sinks. The benefit of the simplified non-discrete approaches is an easily applicable analytical solution. For the discrete approach, a straightforward analytical solution can be found for a steady state, while for an arbitrary time-dependent situation, the particle concentrations need to be solved numerically. Case studies presented in this work demonstrate that the results given by approaches that do not consider the discrete nature of the dynamic processes may be notably distorted. The results of two analytical extrapolation methods were evaluated both in the specific situations they are derived for (an initially monodisperse particle population for one method and steady state for the other) and in other conditions, as both methods have been used in a variety of situations. While the qualitative analytical size distribution can be similar to the discrete result, there may be deviations in both the absolute particle concentration, and its location on the time axis in the case of a time-dependent situation. The magnitude of the deviations depends on the studied situation; the differences often increase with increasing scavenging loss rate, but this is not necessarily always the case. For a time-dependent situation, the deviations were found to be in general larger for shorter particle formation periods. In the studied situations, the differences in the concentrations were around a factor of ten or less to either direction depending on the conditions.

The problem related to the assumption of particles of equal size growing at the same rate is obvious in the free molecular regime: in order for a monodisperse particle population to stay perfectly monodisperse while growing, vapor molecules would need to collide synchronously on all particles at exactly the same moments. This is clearly not realistic, and at least some dispersion is expected.

It must be noted that the results presented here cannot be applied to draw conclusions on a situation where the condensing vapor is known to be volatile. For instance, extrapolating concentrations of larger particles down to an assumed thermodynamical “critical size” using the methods discussed in this study would lead to even greater errors than in the examples shown here; while the evaporation rate of clusters slightly above the critical size is by definition lower than the condensation rate, it may still be significant. The size-dependent particle evaporation rate is likely to be strongly dependent on the properties of the vapor and the particles, and assessing its effect is beyond the scope of this study. Also, situations where the effect of self-coagulation among the particle population can be expected to be non-negligible are outside the range of applicability of traditional extrapolation methods, and these cases always require numerical treatment (see *e.g.* Anttila et al., 2010).

The aim of this work was to examine the differences between the exact discrete and simplified analytical approaches in the simplest possible case of competing condensational growth and particle scavenging. The results demonstrate that in the nanometer size range, obtaining reliable quantitative estimates for the size-dependent particle concentration and related quantities, such as the particle survival probability, requires discrete treatment of the particle population.

Acknowledgments

ERC project 257360-MOCAPAF and the Academy of Finland Center of Excellence program project no. 272041 are acknowledged for funding.

Appendix A

A.1. Solutions for an initially monodisperse distribution with size-independent rate constants

Figure A1 shows the time-dependent particle concentrations in the case of an initially monodisperse distribution for size-independent condensation and loss rate constants $f=10^{-2}\,s^{-1}$ and $S=10^{-4}\,s^{-1}$ obtained by the discrete approach (Eq. (4)), and by the first (Eq. (5)) and second (Eq. (7)) order Taylor series approximations. In these conditions, the second-order approximation follows the discrete result quite well, but the difference between the two slightly increases with increasing S/f ratio. For instance, for $S=10^{-4}\,s^{-1}$, the ratio of the peak concentrations for each particle size given by the second-order approximation and the discrete calculation increases up to 1.23 as the size decreases, and approaches one for larger sizes. When S is increased to $10^{-3}\,s^{-1}$ and $2\times10^{-3}\,s^{-1}$, the relative differences in the peak concentrations are at most 1.27 and 1.31, respectively. However, the fact that the second-order treatment becomes extremely complex for size-dependent rate constants and situations including particle sources limits its applicability in practice.

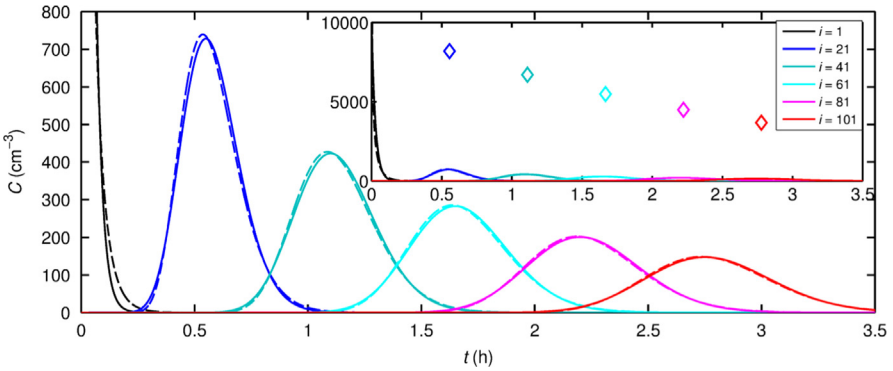

Fig. A1. Time evolution of the concentrations of particles containing 0–100 vapor molecules for an initially monodisperse distribution $C_i\,(t=0)=10^4\,cm^{-3}$ for $i=1$, and $C_i\,(t=0)=0$ for $i>1$ for size-independent condensation and loss rate constants $f=10^{-2}\,s^{-1}$ and $S=10^{-4}\,s^{-1}$. The discrete result (Eq. (4)) is shown by solid lines, and the results obtained by approximating the particle size as a continuous variable considering size derivatives up to the first (Eq. (5)) and second (Eq. (7)) order are depicted with diamonds and dashed lines, respectively. The diamonds are placed at times $\Delta t_{\mathrm{growth},i}$ (Eq. (19)) at which the particles are assumed to reach size i. The inset shows the general view including the first-order result, and the main frame is a zoom to concentrations below 800 cm^{-3}. For figure clarity, only the data for every 20th particle are shown.

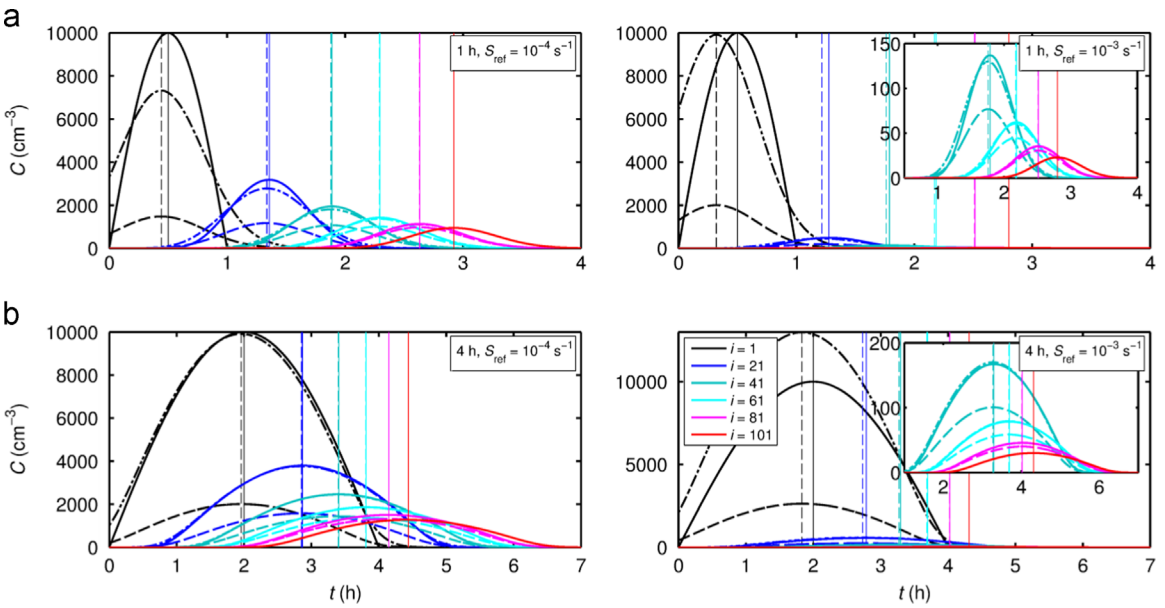

Fig. A2. Particle concentrations solved from the discrete rate equations as a function of time (thick solid lines), and concentrations extrapolated from the largest size studied towards smaller sizes according to the monodisperse mode formula (Eq. (12); thick dashed lines) and the first-order continuous approximation (Eq. (14); thick dash-dotted lines) and shifted by the assumed growth time $\Delta t_{\mathrm{growth},i}$ (Eq. (19)). Explanations for the panels are as in Fig. 3.

A.2. Extrapolation towards smaller sizes for the conditions of Fig. 3

Figure A2 shows the results for extrapolations performed from the discrete solution for the time evolution of the largest size of 100 vapor molecules towards smaller sizes in the conditions of Fig. 3. The differences between the maximum concentrations for individual sizes obtained by the different approaches are of the same order as for the extrapolation from small to large sizes, but here the formation periods of the small sizes, *i.e.* the lengths of time during which the concentration is non-zero, are overestimated by the simplified approaches.

References

Anttila, T., Kerminen, V.-M., & Lehtinen, K. E. J. (2010). Parameterizing the formation rate of new particles: The effect of nuclei self-coagulation. *Journal of Aerosol Science*, *41*, 621–636.

Brock, J. R. (1972). Condensational growth of atmospheric aerosols. *Journal of Colloid and Interface Science*, *39*, 32–36.

Chapman, S., & Cowling, T. G. (1970). *The mathematical theory of nonuniform gases*. Cambridge: University Press.

Clement, C. F., Lehtinen, K. E. J., & Kulmala, M. (2004). Size diffusion for the growth of newly nucleated aerosol. *Journal of Aerosol Science*, *35*, 1439–1451.

Clement, C. F., & Wood, M. H. (1979). Equations for the growth of a distribution of small physical objects. *Proceedings of the Royal Society A*, *368*, 521–546.

Clement, C. F., & Wood, M. H. (1980). Moment and Fokker–Planck equations for the growth and decay of small objects. *Proceedings of the Royal Society A*, *371*, 553–567.

Ehn, M., Thornton, J. A., Kleist, E., Sipilä, M., Junninen, H., & Pullinen, I., et al. (2014). A large source of low-volatility secondary organic aerosol. *Nature*, *506*, 476–479.

Glasoe, W. A., Volz, K., Panta, B., Freshour, N., Bachman, R., & Hanson, D. R., et al. (2015). Sulfuric acid nucleation: An experimental study of the effect of seven bases. *Journal of Geophysical Research: Atmospheres*, *120*, 1933–1950.

Goodrich, F. C. (1964a). Nucleation rates and the kinetics of particle growth I. The pure birth process. *Proceedings of the Royal Society A*, *277*, 155–166.

Goodrich, F. C. (1964b). Nucleation rates and the kinetics of particle growth II. The birth and death process. *Proceedings of the Royal Society A*, *277*, 167–182.

Kerminen, V.-M., Anttila, T., Lehtinen, K. E. J., & Kulmala, M. (2004). Parameterization for atmospheric new-particle formation: Application to a system involving sulfuric acid and condensable water-soluble organic vapors. *Aerosol Science & Technology*, *38*, 1001–1008.

Kerminen, V.-M., & Kulmala, M. (2002). Analytical formulae connecting the 'real' and the 'apparent' nucleation rate and the nuclei number concentration for atmospheric nucleation events. *Journal of Aerosol Science*, *33*, 609–622.

Korhonen, H., Kerminen, V.-M., Kokkola, H., & Lehtinen, K. E. J. (2014). Estimating atmospheric nucleation rates from size distribution measurements: Analytical equations for the case of size dependent growth rates. *Journal of Aerosol Science*, *69*, 13–20.

Korhonen, H., Sihto, S.-L., Kerminen, V.-M., & Lehtinen, K. E. J. (2011). Evaluation of the accuracy of analysis tools for atmospheric new particle formation. *Atmospheric Chemistry and Physics*, *11*, 3051–3066.

Kulmala, M., Kontkanen, J., Junninen, H., Lehtipalo, K., Manninen, H. E., & Nieminen, T., et al. (2013). Direct observations of atmospheric aerosol nucleation. *Science*, *339*, 943–946.

Kulmala, M., Petäjä, T., Nieminen, T., Sipilä, M., Manninen, H. E., & Lehtipalo, K., et al. (2012). Measurement of the nucleation of atmospheric aerosol particles. *Nature Protocols*, *7*, 1651–1667.

Kürten, A., Williamson, C., Almeida, J., Kirkby, J., & Curtius, J. (2015). On the derivation of particle nucleation rates from experimental formation rates. *Atmospheric Chemistry and Physics*, *15*, 4063–4075.

Lee, Y. H., Pierce, J. R., & Adams, P. J. (2013). Representation of nucleation mode microphysics in a global aerosol model with sectional microphysics. *Geoscientific Model Development*, *6*, 1221–1232.

Lehtinen, K. E. J., Dal Maso, M., Kulmala, M., & Kerminen, V.-M. (2007). Estimating nucleation rates from apparent particle formation rates and vice versa: Revised formulation of the Kerminen–Kulmala equation. *Journal of Aerosol Science*, *38*, 988–994.

Noppel, M. (1996). Nucleation in the presence of air ions and aerosol particles. In M. Kulmala, & P. E. Wagner (Eds.), *Nucleation and atmospheric aerosols* (pp. 208–211). Oxford: Pergamon.

Olenius, T., Riipinen, I., Lehtipalo, K., & Vehkamäki, H. (2014). Growth rates of atmospheric molecular clusters based on appearance times and collision-evaporation fluxes: Growth by monomers. *Journal of Aerosol Science*, *78*, 55–70.

Olver, P. J. (2014). *Introduction to partial differential equations*. New York: Springer.

Pich, J., Friedlander, S. K., & Lai, F. S. (1970). The self-preserving particle size distribution for coagulation by Brownian motion-III. Smoluchowski coagulation and simultaneous Maxwellian condensation. *Journal of Aerosol Science*, *1*, 115–126.

Precup, R. (2013). *Linear and semilinear partial differential equations: An introduction*. Berlin: De Gruyte.

Ramabhadran, T. E., Peterson, T. W., & Seinfeld, J. H. (1976). Dynamics of aerosol coagulation and condensation. *AIChE Journal*, *22*, 840–851.

Riipinen, I., Sihto, S.-L., Kulmala, M., Arnold, F., Dal Maso, M., & Birmili, W., et al. (2007). Connections between atmospheric sulphuric acid and new particle formation during QUEST III–IV campaigns in Heidelberg and Hyytiälä. *Atmospheric Chemistry and Physics*, *7*, 1899–1914.

Schobesberger, S., Junninen, H., Bianchi, F., Lönn, G., Ehn, M., & Lehtipalo, K., et al. (2013). Molecular understanding of atmospheric particle formation from sulfuric acid and large oxidized organic molecules. *Proceedings of the National Academy of Sciences of the United States of America*, *110*, 17223–17228.

Shi, G., & Seinfeld, J. H. (1990). Homogeneous nucleation in the presence of an aerosol. *Journal of Colloid and Interface Science*, *135*, 252–258.

Sihto, S.-L., Kulmala, M., Kerminen, V.-M., Dal Maso, M., Petäjä, T., & Riipinen, I., et al. (2006). Atmospheric sulphuric acid and aerosol formation: Implications from atmospheric measurements for nucleation and early growth mechanisms. *Atmospheric Chemistry and Physics*, *6*, 4079–4091.

Spracklen, D. V., Carslaw, K. S., Kulmala, M., Kerminen, V.-M., Mann, G. W., & Sihto, S.-L. (2006). The contribution of boundary layer nucleation events to total particle concentrations on regional and global scales. *Atmospheric Chemistry and Physics*, *6*, 5631–5648.

Telford, J. W. (1955). A new aspect of coalescence theory. *Journal of Meteorology*, *12*, 436–444.

Twomey, S. (1964). Statistical effects in the evolution of a distribution of cloud droplets by coalescence. *Journal of the Atmospheric Sciences*, *21*, 553–557.

Wang, J., McGraw, R. L., & Kuang, C. (2013). Growth of atmospheric nano-particles by heterogeneous nucleation of organic vapor. *Atmospheric Chemistry and Physics*, *13*, 6523–6531.

Weber, R. J., Marti, J. J., McMurry, P. H., Eisele, F. L., Tanner, D. J., & Jefferson, A. (1997). Measurements of new particle formation and ultrafine particle growth rates at a clean continental site. *Journal of Geophysical Research D: Atmospheres*, *102*, 4375–4385.

Zhang, R., Suh, I., Zhao, J., Zhang, D., Fortner, E. C., & Tie, X., et al. (2004). Atmospheric new particle formation enhanced by organic acids. *Science*, *304*, 1487–1490.